

CAN DUST INJECTED BY SNe EXPLAIN THE NIR-MIR EXCESS IN YOUNG MASSIVE STELLAR CLUSTERS?

SERGIO MARTÍNEZ-GONZÁLEZ¹, RICHARD WÜNSCH¹, JAN PALOUŠ¹

ACCEPTED TO APJ: May 23rd, 2017

ABSTRACT

We present a physically-motivated model involving the different processes affecting supernova dust grains as they are incorporated into the thermalized medium within young massive star clusters. The model is used to explain the near- to mid-infrared (NIR-MIR) excess found in such clusters and usually modeled as a blackbody with temperature $\sim (400 - 1000)$ K. In our approach, dust grains are efficiently produced in the clumpy ejecta of core-collapse supernovae, fragmented into small pieces ($\lesssim 0.05 \mu\text{m}$) as they are incorporated into the hot and dense ISM, heated via frequent collisions with electrons and the absorption of energetic photons. Grains with small sizes can more easily acquire the high temperatures (~ 1000 K) required to produce a NIR-MIR excess with respect to the emission of foreground PAHs and starlight. However, the extreme conditions inside young massive clusters make difficult for these small grains to have a persistent manifestation at NIR-MIR wavelengths as they are destroyed by efficient thermal sputtering. Nevertheless, the chances for a persistent manifestation are increased by taking into account that small grains become increasingly transparent to their impinging ions as their size decreases. For an individual SN event, we find that the NIR-MIR excess last longer if the time required to incorporate all the grains into the thermalized medium is also longer, and in some cases, comparable to the characteristic interval between supernova explosions. Our models, can successfully explain the near-infrared excesses found in the star clusters observed in M33 (Relaño et al. 2016) assuming a low heating efficiency and mass-loading. In this scenario, the presence of the NIR-MIR excess is an indication of efficient dust production in SNe and its subsequent destruction.

1. INTRODUCTION

It has been extensively shown, both theoretically and observationally, that the ejecta of core-collapse supernovae (SN) meet the appropriate conditions for the efficient condensation of refractory elements onto massive quantities of dust (see for example Cernuschi et al. 1967; Moseley et al. 1989; Suntzeff & Bouchet 1990). From the observational perspective, SN 1987A provides the most compelling evidence so far for the condensation of dust in the ejecta of a supernova remnant (SNR), producing $\sim (0.7 - 0.9) M_{\odot}$ of dust during the first ~ 25 years after the explosion of a progenitor star with initial mass $\sim 19 M_{\odot}$ (Indebetouw et al. 2014; Matsuura et al. 2014). More recently, De Looze et al. (2017) and Bevan et al. (2016) have also derived a large mass of dust condensed in the clumpy ejecta of Cassiopeia A, with values ranging from $\sim (0.4 - 0.6) M_{\odot}$ in the former study and $\sim 1.1 M_{\odot}$ in the latter analysis. From the theoretical point of view, one can expect that a single supernova would be able to condense $\sim (0.1 - 3.1) M_{\odot}$ of dust out of progenitors in a mass range $\sim (13 - 80) M_{\odot}$ (Todini & Ferrara 2001; Nozawa et al. 2003). The presence of inhomogeneities in SN ejecta (“clumpiness”), as observed in many SNRs, favors the formation of large quantities of dust (Biscaro & Cherchneff 2016) and the coagulation of small grains into larger aggregates (Sarangi & Cherchneff 2015). That is not the end of the story, as these dust grains might be heavily eroded by the action of thermal and kinetic sputtering and, in the presence of turbulence, disrupted in grain-grain collisions

as they are reached by the supernova reverse shock.

In this respect, the study of isolated SNRs evolving in diffuse low-temperature media has given insights on the dust mass fraction which is able to survive the passage of the reverse shock and make their way into the ISM (see, for example Bianchi & Schneider (2007); Nozawa et al. (2007); Marassi et al. (2015); Micelotta et al. (2016); Bocchio et al. (2016) for theoretical estimates and Lau et al. (2015); Ghavamian & Williams (2016); Lakićević et al. (2015) for observational constraints). These studies agree that such fraction would lie between 0 (completely destroyed) and 0.8 depending on the ISM density and the mixing efficiency of the ejecta.

1.1. SNRs evolving in SSCs

From the occurrence of a supernova explosion, the ISM is structured as follows: a region in which the ejecta expands freely; eventually two shocks are formed, a reverse shock (RS), which thermalizes the ejecta, and a leading shock (LS), which thermalizes the ISM; the shocked ejecta region is separated by a contact discontinuity from the matter swept-up by the leading shock. The thermalization of the kinetic energy is enhanced in young stellar clusters as stellar winds and supernova shells randomly collide and merge, thus creating a large central overpressure which results in the launching of a strong star cluster wind with temperatures $\gtrsim 10^6$ K and densities $\sim (1 - 1000) \text{cm}^{-3}$ (Chevalier & Clegg 1985; Silich et al. 2004, 2011; Wunsch et al. 2011).

Thermal sputtering, promoted by the passage of the reverse shock, would lead to a size distribution favoring big grains ($\gtrsim 0.05 \mu\text{m}$), as can be noted from the characteristic (graphite/silicate) grain lifetime against thermal sputtering in a hot gas, τ_{sput} :

¹ Astronomical Institute, Academy of Sciences of the Czech Republic, Boční II 1401-2a, Prague, Czech Republic; martinez@asu.cas.cz

$$\tau_{\text{sput}} = \frac{a}{|\dot{a}|} = 7 \times 10^5 \frac{a(\mu\text{m})}{n(\text{cm}^{-3})} \left[\left(\frac{T}{2 \times 10^6 \text{ K}} \right)^{-2.5} + 1 \right], \quad (1)$$

in units of years. In the above equation a is the grain radius, \dot{a} is the rate of decrease of the grain radius (Draine & Salpeter 1979; Tielens et al. 1994; Tsai & Mathews 1995), n is the gas number density, and T is the gas temperature. With ambient conditions $T = 10^7$ K and $n = 10 \text{ cm}^{-3}$, a grain with radius $a = 0.005 \mu\text{m}$ would be completely eroded in ~ 350 years, while for $a = 1 \mu\text{m}$, it would take $\sim 7.1 \times 10^4$ years. However, shocks in a magnetized medium may also enhance the occurrence of frequent grain-grain collisions (Jones et al. 1996). This can occur if the majority of grains reside in dense clumps and they move at high speeds relative to each other as a result of magnetohydrodynamic turbulence (see the discussion in Section 2.2). This might imply that the population of small grains can be replenished from the shattering of long-living big grains. If this is the case, the post-shock size distribution will have an excess of small grains. Evidence in the $\sim 10^4$ year-old galactic supernova remnant *Sgr A East* (Lau et al. 2015) seems to point to an enhanced mass ratio between small grains and large grains (with characteristic sizes $\sim 0.001 \mu\text{m}$ and $\sim 0.04 \mu\text{m}$, respectively), with values as high as 0.59 and 0.90 in the post-shock south clump and north regions.

As it was shown by Martínez-González et al. (2016) (hereafter MTS16), the evolution of the grain size distribution promoted by thermal sputtering could greatly affect the appearance of the infrared spectral energy distributions (IR SEDs) of young stellar clusters, with the population of small grains playing a major role at NIR-MIR wavelengths. The importance of small grains ($\lesssim 0.05 \mu\text{m}$) on the emission properties of dusty media lies on their low heat capacities (as the heat capacity scales as $\sim a^3$). From the action of either electron-grain collisions (promoted in the hot and dense plasma streaming out as a star cluster wind) or the absorption of energetic photons (given their ample supply from a collection of hundreds or thousands of massive stars, Takeuchi et al. 2003), small grains are more and more affected by stochastic temperature fluctuations compared to their bigger counterparts, provoking that they acquire temperatures from a few Kelvin up to $\sim 10^3$ K, thus leaving their imprint at near-infrared (NIR) and mid-infrared (MIR) wavelengths.

However, the conditions which allow collisional heating in a hot plasma, also promote thermal sputtering, with a greater impact on small grains. Arendt et al. (2010) modeled the spectra of the Puppis A Supernova Remnant and showed that dust emission at short wavelengths ($\lambda \leq 20 \mu\text{m}$) is significantly reduced in the post-shock region (relative to the pre-shock region) given an efficient small grain destruction.

NIR-MIR emission ($\sim 1 - 5 \mu\text{m}$), in excess to that of starlight and Polycyclic Aromatic Hydrocarbons (PAHs), has been observed in many nearby H II regions surrounding individual young stellar clusters, as in a number of the more than one hundred H II regions in M33 which proper-

ties have been thoroughly studied by (Relaño et al. 2013, 2016) (like NGC 604 and NGC 595, to name the most prominent examples) and in individual clusters in SBS 0335-052E (Reines et al. 2008). In fact, Relaño et al. (2016) and Reines et al. (2008) required an additional ~ 1000 -K blackbody component of “uncertain origin” to fit their observed IR SEDs.

Similar excesses, more prevalent in the MIR, have also been observed in a number of blue compact dwarf galaxies (e.g: I Zw 18, II Zw 40, Mrk 930 and Haro 11 (Rémy-Ruyer et al. 2015; Vanzi et al. 2000; Izotov et al. 2014)). Therefore, these observations not only point to the existence of a very hot dust component (~ 400 - 1000 K), but also give compelling evidence for the presence of a persistent (i.e. long-living and/or constantly replenished) population of small grains associated to young stellar clusters.

From these motivations, here we advocate that a population of SN-condensed small grains, heated by the intense radiation field emerging from the cluster and frequent electronic collisions in the thermalized ejecta, is responsible for the observed NIR-MIR excesses in young massive clusters, in particular in the case of the young massive clusters in M33. For this purpose, we have considered a number of physical effects which might prolong the emergence of the NIR-MIR excess, e.g. a quick replenishment and mitigated destruction of the population of small grains.

The paper is organized as follows: in Section 2 we introduce our star cluster and star cluster wind models (subsection 2.1), the consideration of grain processing in clumpy SN ejecta (2.2), the formulation of the supernova dust injection process and its relevant timescales are presented (subsection 2.3). In Section 3 we give the reasons to apply our model to the infrared spectral energy distributions to the most prominent H II regions in M33 and review some of their relevant properties (stellar mass, spectral indexes, age) obtained from the literature; we also briefly discuss the treatment of the additional dust components, other than the newly-produced grains, required to fit the observed IR SEDs in the whole infrared regime (subsection 3.1). Section 4 deals with the results of our models and the requirements of the model to work. Our results are presented at different evolutionary times. In Section we discuss the relative importance of other dust sources compared to SN dust. The summary of the main ingredients of the model are presented in Section 6, while our conclusions appear in Section 7.

2. HOT DUST WITHIN THE STAR CLUSTER

2.1. Star Cluster Wind Model

We focus on coeval young massive stellar clusters with ages 4-6 Myr, i.e. at the start of their supernova era (with the first SN occurring at ~ 3.5 Myr, e.g. Krause et al. 2013; Martínez-González et al. 2014; Wünsch et al. 2017). At ~ 6 Myr, all stars with masses $\geq 40 M_{\odot}$ should have exploded as supernovae (Meynet & Maeder 2003). For simplicity, the SN explosions are considered to occur at the very center of spherically-symmetric young star clusters with a Schuster stellar density distribution of the form $\rho_* \propto [1 + (r/R_c)^2]^{-\beta}$, where β is taken to be 1.5, r is the distance from the cluster center, R_c is the core ra-

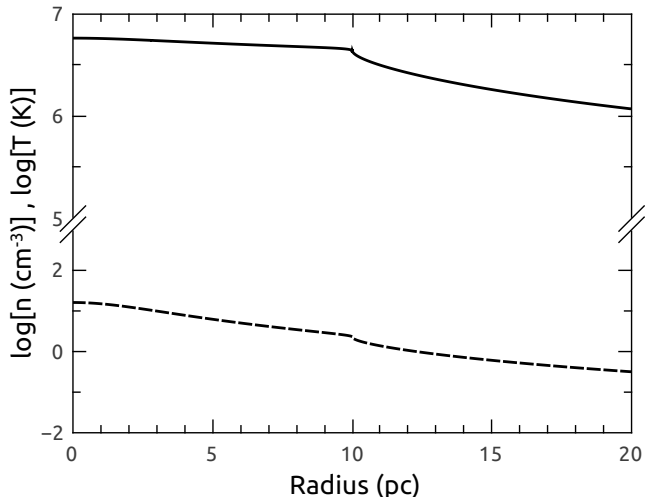


FIG. 1.— The radial distribution of temperature and density in the star cluster as calculated from our hydrodynamical model (Silich et al. 2011; Palouš et al. 2013). The upper and lower curves correspond to the calculated temperature and density, respectively, for a cluster with $L_{SC} = 1.7 \times 10^{40}$ erg s $^{-1}$, $R_c = 3$ pc, $R_{SC} = 10$ pc and $V_{\eta\infty} = 630$ km s $^{-1}$. This model is later applied to the case of the central cluster in NGC 604 (see Section 3). Note the axis break and the change of units in the upper and lower regions of the plot.

dius and R_{SC} is the star cluster truncation radius. We calculate the gas number density and temperature inside the star cluster by making use of the model thoroughly discussed in Silich et al. (2011) and Palouš et al. (2013) which solves the set of hydrodynamic equations for the stationary flow driven by stellar winds and supernova explosions. Our models include the effects of gas (Raymond et al. 1976) and dust radiative cooling (Dwek 1987; Tenorio-Tagle et al. 2013, 2015b; Martínez-González et al. 2016). The star cluster mechanical luminosity, L_{SC} , and the stellar mass of the cluster, M_{SC} , are related as $L_{SC} = 3 \times 10^{39} (M_{SC}/10^5 M_{\odot})$ erg s $^{-1}$ (Leitherer et al. 1999). The mechanical energy is treated as a constant due to the short timescales, on the order of thousands of years, investigated in this work. Within the cluster, mass is reinserted via stellar winds and SN explosions at a rate $\dot{M} = 2L_{SC}/V_{A\infty}^2$, where $V_{A\infty}$ is the adiabatic wind terminal speed.

One can also consider two important parameters: heating efficiency (η_{he}) and mass loading (η_{ml}). The former represents the fraction of L_{SC} which is converted into the thermal energy of the wind (see e.g. Silich et al. 2007). The latter arises under the condition of a non-negligible mass of gas left over from star formation which is incorporated into the star cluster wind at a rate $\dot{M}_{inj} = (1 + \eta_{ml})\dot{M}$ (see e.g. Wunsch et al. 2011). After the consideration of η_{he} and η_{ml} , the value of the wind terminal speed changes to $V_{\eta\infty} = V_{A\infty} [\eta_{he}/(1 + \eta_{ml})]^{1/2}$. In Figure 1, we show the radial distribution of temperature and density of the wind in a star cluster with $L_{SC} = 1.7 \times 10^{40}$ erg s $^{-1}$, R_c and R_{SC} equal to 3 and 10 pc respectively, and $V_{\eta\infty} = 630$ km s $^{-1}$. This model is later applied to the case of the central cluster in NGC 604 (see Section 3).

Given a low heating efficiency, grain thermal sputtering is reduced as a consequence of a lower temperature in the

shocked wind, alleviating the destruction of the population of small grains necessary to explain the NIR-MIR excesses. In favor of a low heating efficiency, first proposed by Smith et al. (2006) and Larsen et al. (2006), one can mention the work of Silich et al. (2007, 2009), who studied several young clusters in the central zone of M82. They found that the observed sizes and expansion velocities of the associated H II regions are not consistent with the standard bubble model (Weaver et al. 1977) which might be the result of a low heating efficiency ($\lesssim 0.1$).

2.2. Grain Processing in Clumpy Ejecta

In star clusters, SN-condensed grains residing in dense clumps might be efficiently accelerated by the magnetohydrodynamic (MHD) turbulence sustained by massive stars as shown by Hirashita et al. (2010). For instance, they found that a grain (silicate or carbonaceous) with radius $0.1 \mu\text{m}$ in an ionized warm medium with density between 1 and 10 cm^{-3} moves at a speed of a few km s $^{-1}$ with respect to another grain with radius $0.01 \mu\text{m}$ (see their Figure 1). Moreover, as the clumps in the ejecta are traversed by the reverse shock, the grains would experience a further size-dependent acceleration as they gyrate along the compressed magnetic field lines (Yan et al. 2004; Shull 1977).

On this basis, one can anticipate the relevance of grain-grain collisions and the modification of the grain size distribution in clumpy SN within star clusters. If we assume that all the newly-condensed grains reside in clumps with radius 500 AU and a mass of dust per clump $M_{dcl} = 10^{-6} M_{\odot}$ (average values for the dusty globules in the Crab Nebula, Grenman et al. 2017). Then, the average dust number density inside each clump is

$$\langle n_d \rangle = \frac{3M_{dcl}}{4\pi \langle m_d \rangle R_{cl}^3}, \quad (2)$$

where $\langle m_d \rangle$ is the mean mass per grain. For a size distribution of the grains in the unshocked clumps characterized by a power-law, $\sim a^{-\alpha}$ with $\alpha = 3.8$ (Temim & Dwek 2013, ²) and lower and upper limits $a_{min} = 0.001 \mu\text{m}$ and $a_{max} = 0.1 \mu\text{m}$, respectively, $\langle m_d \rangle$ is $\approx 2.9 \times 10^{-19}$ g (for a grain density equal to 3.3 g cm^{-3}), thus the average grain size is $\langle a \rangle \approx 0.0027 \mu\text{m}$ and $\langle n_d \rangle \approx 3.9 \times 10^{-3} \text{ cm}^{-3}$.

The timescale for an encounter between a grain with radius a , and an average grain of radius $\langle a \rangle$ in a clump is

$$\Delta t_{coll} = [\pi(a + \langle a \rangle)^2 \langle n_d \rangle \delta v]^{-1}, \quad (3)$$

where δv is the mean relative velocity between grains. If δv is higher than 2.7 km s^{-1} for silicate and 1.2 km s^{-1} for graphite grains (Jones et al. 1996), as it is in the case of the MHD turbulence predicted by Hirashita et al. (2010), then the grain population is effectively influenced by shattering during the lifetime of the clumps. For instance, if $\delta v \approx 5 \text{ km s}^{-1}$, a silicate grain with radius $0.1 \mu\text{m}$ will encounter another grain every 14 days.

² Temim & Dwek (2013) found that the grain size distribution for the Crab Nebula is characterized by a power-law index between -3.5 and -4.0

The lifetime of individual ejecta clumps is largely defined by the propagation of the reverse shock across them, leading to their fragmentation and rapid destruction. The dynamical time for this process has been estimated by Micelotta et al. (2016). For a clump with radius $R_{cl} \sim 500$ AU, a density contrast between the clump and the smooth ejecta ~ 100 , and the (attenuated) propagation velocity of the shock within the clump $V_{cl} \approx 150$ km s $^{-1}$, the clump would be destroyed in $t_{dest} = 3.5R_{cl}/V_{cl} \approx 55$ years. This is a very short time compared to the crossing time of the reverse shock through the whole ejecta ($\lesssim 3\%$ in all our calculations, see Section 2.3), but also large compared to Δt_{coll} . The implication is that by the time when thermal sputtering commences to act in the thermalized ejecta, the grain size distribution has already been shifted towards smaller grains. One can then assume that grains with radius ≥ 0.05 μm have all been shattered, thus producing an excess of grains with radius ≤ 0.001 μm . From the above considerations, in our calculations we have taken the grain size distribution immediately after clump destruction to have the form $\sim a^{-\alpha}$ ($\alpha = 3.8$) with lower and upper limits $a_{min} = 0.0005$ μm and $a_{max} = 0.05$ μm .

In characterizing the emission from grains residing in unshocked clumps, we consider that silicate and graphite grains (assumed to be produced in equal proportions) are only heated by the absorption of the radiation field emerging from the cluster, whereas grains in the thermalized medium (see next Section) are also subject to heating induced by collisions with free electrons.

2.3. Dust Injection into the Thermalized Medium

We follow the evolution of the graphite and silicate grain populations under the action of thermal sputtering in a similar manner (albeit more physically motivated) as MTS16. Once the gas from the ejecta is thermalized, its temperature and density is similar to that of the shocked star cluster wind, and thus they are considered to be the same medium. In the subsequent, we will refer to the SN ejecta and the cluster wind simply as the thermalized medium.

Dust injection into the thermalized medium starts once individual clumps in the ejecta are destroyed, and finishes when all the ejecta is thermalized (at $t = \tau_{inj}$). This occurs in a timescale (in units of years) given by Tang & Wang (2009) (see also Reynolds & Chevalier 1984) for a supernova remnant evolving in a hot medium:

$$\tau_{inj} \simeq 10^4 \left(\frac{\rho}{\rho_s} \right)^{-1/3} \left(\frac{M_{ej}}{1.4 M_\odot} \right)^{5/6} \left(\frac{E_{SN}}{10^{51} \text{ erg}} \right)^{-1/2}, \quad (4)$$

where $\rho = 1.4m_H n$ is the gas density, m_H is the H mass, $\rho_s = 1.67 \times 10^{-26}$ g cm $^{-3}$, M_{ej} is the ejecta mass and E_{SN} is the kinetic energy of the ejecta. At τ_{inj} , the radius of the leading shock can be expressed as:

$$R_{LS}(\tau_{inj}) = \xi \left(\frac{E_{SN} \tau_{inj}^2}{\rho} \right)^{1/5} {}_2F_1 \left(\frac{-3}{5}, \frac{2}{5}; \frac{7}{5}; -\frac{\tau_{inj}}{t_c} \right), \quad (5)$$

where ${}_2F_1$ is the Gauss hypergeometric function

which accounts for a non-negligible ambient pressure (Tang & Wang 2005), ξ is equal to 1.15 (for an ideal gas with a ratio of specific heats $\gamma = 5/3$) and t_c is defined as:

$$t_c = \left[\left(\frac{2}{5} \xi \right)^5 \frac{E_{SN}}{\rho c_s^5} \right]^{1/3}, \quad (6)$$

with c_s representing the ambient medium sound speed. For reference, if $n = 5$ cm $^{-3}$, $T = 5.5 \times 10^6$ K, $M_{ej} = 8 M_\odot$ and $E_{SN} = 10^{51}$ erg, the injection timescale would be $\tau_{inj} \sim 3820$ years when the leading shock would have reached $R_{LS} \sim 4.90$ pc.

From the consideration of dust being incorporated into the thermalized medium and the action of thermal sputtering, the grain size distribution, $\partial n_i / \partial a$ (where n_i is the grain number density of each dust species), evolves with time from the continuity equation (Laor & Draine (1993); Yamada & Kitayama (2005):

$$\dot{a} \frac{\partial}{\partial a} \left(\frac{\partial n_i}{\partial a} \right) + \frac{\partial}{\partial t} \left(\frac{\partial n_i}{\partial a} \right) = A_i^{(m)} a^{-\alpha} / \tau_{inj}^{(m)}, \quad (7)$$

if $t \leq \tau_{SN}^{(m)} + \tau_{inj}^{(m)}$, where α is the index of the dust size distributions immediately after injection into the thermalized medium, $\tau_{inj}^{(m)}$ is the injection timescale for the m -supernova event which occurs at $t = \tau_{SN}^{(m)}$. The normalization constants, $A_i^{(m)}$ (cm $^{\alpha-4}$), are given by:

$$A_i^{(m)} = \frac{f_i M_{dSN}^{(m)} / V_{SC}}{\int_{a_{min}}^{a_{max}} \frac{4}{3} \pi \rho_{gr} a^{3-\alpha} da}, \quad (8)$$

where ρ_{gr} is the grain density, f_i is the species mass fraction, $M_{dSN}^{(m)}$ is the total mass of dust formed/injected in a single supernova and V_{SC} is the star cluster volume.

The constants $A_i^{(m)}$, are zero until $t = \tau_{SN}^{(m)}$. If the reverse shock has already reached all the dust produced by the m -supernova ($t > \tau_{SN}^{(m)} + \tau_{inj}^{(m)}$), i.e. dust injection has ceased, the right-hand term in equation (7) is set to zero. General solutions of equation (7) corresponding to j dust injections are given by (MTS16):

$$\frac{\partial n_i}{\partial a} = \sum_{m=1}^j \frac{A_i^{(m)}}{\tau_{inj}^{(m)} \dot{a}} \left\{ \frac{a^{-\alpha+1}}{(-\alpha+1)} - \frac{[a - \dot{a}(t - \tau_{SN}^{(m)})]^{-\alpha+1}}{(-\alpha+1)} \right\}, \quad (9)$$

for $t \leq \tau_{SN}^{(m)} + \tau_{inj}^{(m)}$, and after the m -dust injection (for $t > \tau_{SN}^{(m)} + \tau_{inj}^{(m)}$):

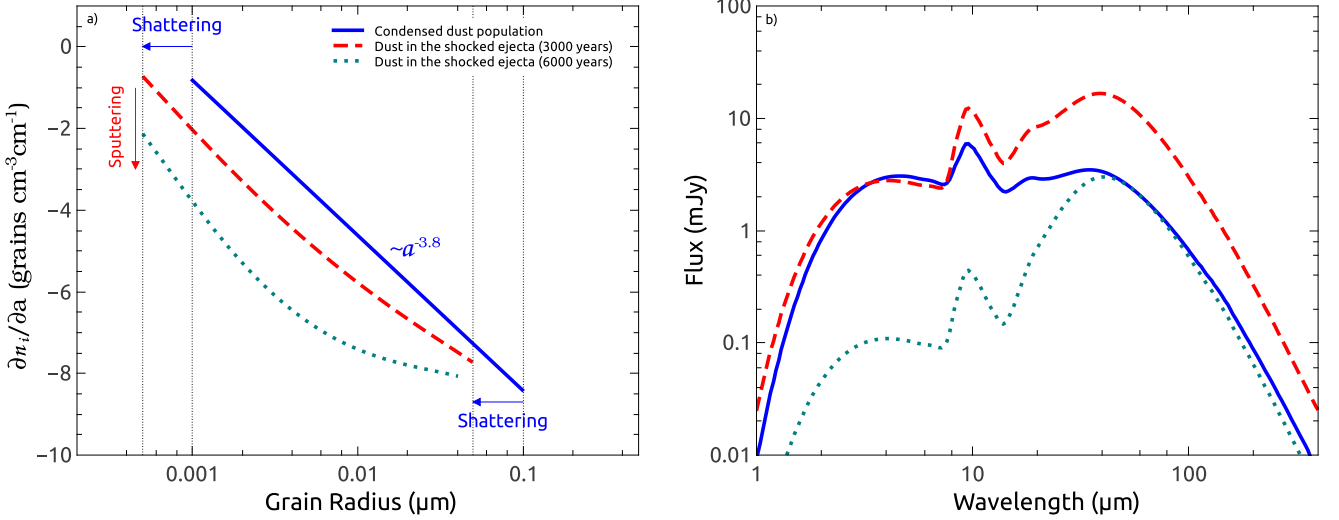


FIG. 2.— The Evolution of the Grain Size Distribution and the associated IR emission. Panel a: The blue solid line displays the size distribution of the condensed dust population. The red-dashed (green-dotted) line corresponds to the size distribution associated to dust grains already incorporated into the thermalized medium at 3000 (6000) years after the dust injection started. Grain shattering shifts the distribution towards smaller grains ($a_{min} = 0.0005 \mu\text{m}$ and $a_{max} = 0.05 \mu\text{m}$, indicated by blue arrows) while thermal sputtering lowers it (indicated by a red arrow) and changes its slope. Grains smaller than (bigger than) $\sim 0.005 \mu\text{m}$ are less (more) affected by ionic collisions and thus the size distribution is not simply described by a power-law. The upper and lower limits of the size distributions are marked with dotted vertical lines. Panel b shows the IR emission associated to the grain size distributions presented in panel a (see the text for the description of the input model parameters).

$$\frac{\partial n_i}{\partial a} = \sum_{m=1}^j \frac{A_i^{(m)}}{\tau_{inj}^{(m)} \dot{a}} \left\{ \frac{[a - \dot{a}(t - \tau_{SN}^{(m)} - \tau_{inj}^{(m)})]^{-\alpha+1}}{(-\alpha+1)} - \frac{[a - \dot{a}(t - \tau_{SN}^{(m)})]^{-\alpha+1}}{(-\alpha+1)} \right\}. \quad (10)$$

The interstellar radiation field emerging from the star cluster, J_λ , is characterized by multiples, U , of the solar neighborhood radiation field, J_λ^{NBH} (Mathis et al. 1983). The infrared flux per unit wavelength, produced by a population of dust grains with the same chemical composition, from a source located at distance D_{SC} , is given by:

$$f_\nu = \left(\frac{1.4 m_H Z_d N_H}{\rho_d} \right) \pi \Omega_{SC} \times \int_{a_{min}}^{a_{max}} \int_0^\infty a^2 \frac{\partial n_i}{\partial a} Q_\nu(a) B_\nu(T_d) G(a, T_d) dT_d da, \quad (11)$$

in units $\text{erg s}^{-1} \text{cm}^{-2} \text{Hz}^{-1}$ (Dwek & Arendt 1992). In the above equation, N_H is the hydrogen column density, ρ_d is the size-averaged grain density, Ω_{SC} is the solid angle subtended by the cluster, T_d is the dust temperature, $G(a, T_d)$ is the dust temperature distribution resulting from stochastic temperature fluctuations produced by both, photon absorptions and electron-grain collisions (see Guhathakurta & Draine 1989; Dwek 1986), $Q_\nu(a)$ is the dust absorption efficiency and B_ν is the Planck function. Additionally, Z_d is the time-dependent dust-to-gas mass ratio (MTS16).

After the dusty clumps are reached by the RS, frequent

grain-grain collisions induced by the high grain density inside the clump and the relative motion of the grains in a turbulent ejecta, lead to the very quick fragmentation of the large grains into smaller pieces, thus shifting the size distribution towards smaller grains. Once the clumps are disrupted, shattering is no longer efficient and thermal sputtering dominates the evolution of the grain size distribution according to equations (9) and (10).

However, we have made use of the size-dependent correction to the sputtering yield (the number of atoms removed from a grain after a collision with an energetic particle) as prescribed by Serra Díaz-Cano & Jones (2008) (approximated by the formula given by Bocchio et al. 2012 and averaged by the Maxwell-Boltzmann energy distribution) in order to consider more realistic sputtering rates. This correction has the ability of increasing the derived sputtering yields for medium-sized and big dust grains, while reducing it for very small grains as they become transparent to the more energetic incident ions, thus mitigating their destruction. The latter effect results as the implantation depth of the incident ion (the characteristic radius at which the ion is stopped), becomes larger than the grain diameter (for sufficiently energetic particles, see equation A.2 in Bocchio et al. 2012). Hence, the resultant grain size distribution is no longer described by a simple power-law.

Figure 2 (panel a) presents the evolution of the size distribution of a population of $0.1 M_\odot$ of dust injected into the intracluster medium. Initially, the size distribution (just after grain condensation) is characterized by a power-law $\sim a^{-\alpha}$ with $\alpha = 3.8$, $a_{min} = 0.001 \mu\text{m}$ and $a_{max} = 0.1 \mu\text{m}$. The grain population in this case is heated by a radiation field 2×10^5 times that of the solar neighborhood value (Mathis et al. 1983). Panel a also shows the size distributions corresponding to grains already injected into the thermalized medium, with number density 2.5cm^{-3} and temperature $2.6 \times 10^6 \text{K}$, at $t = 3000$ and

6000 years.

Panel b in Figure 2 displays the IR emission associated to the grain population depicted in panel a. There is a strong NIR-MIR emission from dust heated by starlight in the pre-shocked ejecta which can account for the observed NIR-MIR excess. However, their emission will be rapidly overcome by that of the dust in the post-shock region. Given that the small grains are rapidly destroyed by thermal sputtering, the NIR part of the emission will be greatly reduced after a few thousand years.

As mentioned before, we restrict our models to the case of supernovae occurring at (or very close to) the center of the star cluster. In the case when this assumption is relaxed, off-centered supernova blast waves would be evolving in the steep density gradient expected at large radii in the cluster, leading to the blowout and rapid loss of energy of the ejecta (Tenorio-Tagle et al. 2015a; Silich & Tenorio-Tagle 2017) and the release of the SN products out of the stellar cluster, possibly including a non-negligible amount of dust grains. Finally, although thermal sputtering may produce grains with radii $\leq 0.0005 \mu\text{m}$, these grains are removed from all our calculations as they are considered completely sputtered.

3. THE STAR CLUSTERS IN M33

With the considerations expressed in the prior sections, we have applied our model to the observed IR SEDs of the M33 clusters (located at a distance $\sim 817 \pm 58$ kpc Freedman et al. 2001), in particular to the prominent regions NGC 604, NGC 595, NGC 588, and NGC 592 (regions 98, 44, 7, 25 in the Relaño et al. (2016) sample, respectively). Our intention is not to provide best fitting models to the observed IR SEDs; rather, we aim to show that a population of newly-produced supernovae grains, subject to the extreme prevailing conditions in young massive clusters, is able to explain the NIR-MIR excesses observed in such objects. We selected these four regions, because they all have reliable estimates of their stellar masses (Relaño et al. 2010) and have experienced recent supernova activity as can be inferred from their relatively flat spectral indexes (Tabatabaei et al. 2007; Yang et al. 1996; Gordon et al. 1993, see Table 1), which is interpreted as non-thermal (synchrotron) emission from supernova remnants.

In Table 1 we present the stellar masses for the four regions, their spectral indexes (denoted as ψ), the total number of stars in the respective cluster, the number of massive stars with masses $\geq 40 M_{\odot}$, the average interval between successive supernova explosions ($\langle \Delta\tau_{SN} \rangle$, the inverse of the average supernova rate), as predicted by the Geneva evolutionary tracks (Meynet et al. 1994) implemented in the Starburst99 synthesis model (Leitherer et al. 1999) for a 4-Myr star cluster and a Kroupa initial mass function (indexes -1.3 and -2.3) with lower and upper cut-off mass of $0.1 M_{\odot}$ and $100 M_{\odot}$, respectively, a turn-off mass at $0.5 M_{\odot}$ and metallicity $Z=0.4Z_{\odot}$.

From the consideration of star clusters with masses $\lesssim 10^5 M_{\odot}$, the obtained dust injection timescales represent only a minor fraction of the interval between supernova explosions, making the replenishment of grains difficult. This is why we expect that some important fraction of these clusters (with masses similar to NGC 588 and NGC 592 or lower) should present a marginal or non-existent NIR-

TABLE 1
CLUSTER PROPERTIES

| Region | M_{SC} ($10^4 M_{\odot}$) | ψ - | No. of Stars - | No. of Stars ($\geq 40 M_{\odot}$) | $\langle \Delta\tau_{SN} \rangle$ years |
|---------|----------------------------------|-------------|-------------------|---|--|
| NGC 604 | 56.8 | 0.12 | 6.5×10^5 | 650 | 3800 |
| NGC 595 | 22.4 | 0.07 | 2.6×10^5 | 250 | 8250 |
| NGC 588 | 6.86 | 0.00 | 7.9×10^4 | 80 | 31000 |
| NGC 592 | 3.98 | 0.13 | 4.6×10^4 | 45 | 50000 |

NOTE. — The Table presents the stellar masses of the selected star clusters obtained by Relaño et al. (2010), spectral indexes as estimated by Tabatabaei et al. (2007). For the average interval between supernova explosions we ran a Starburst99 model with a standard Kroupa Initial Mass Function with metallicity $Z=0.4Z_{\odot}$, and Geneva evolutionary tracks (Meynet et al. 1994) with no rotation.

MIR excess with respect to the emission from PAHs. In such cases another problem arises; the typical mass of a SN ejecta (in our case assumed to be $5 M_{\odot}$, see e.g. Yadav et al. 2016) becomes comparable to the gas mass enclosed in the star cluster volume. If this is the case, the capture of the SN ejecta is not achieved and a smooth cluster wind is not developed; rather the supernova explosions behave as isolated events (Sharma et al. 2014) where the dust content is diluted in a larger volume and thermalization is inefficient. To overcome this problem, it is necessary not only to consider a low heating efficiency to reduce the effects of thermal sputtering, but also the effect of mass loading in the stellar wind to warrant that mass enclosed inside R_{SC} is always significantly larger than the mass ejected by a single supernova. For this reason, our models for NGC 588 and NGC 592 include mass loading, however, in conservative values ($\eta_{ml} = 1$).

The hydrodynamical model for NCG 604, consists of a star cluster with a mechanical luminosity $\sim 1.71 \times 10^{40}$ erg s^{-1} , with dimensions given by $R_c = 3$ pc and $R_{SC} = 10$ pc (which give a half-mass radius $R_{HM} = 5.4$ pc), an average interval between successive supernova explosions ~ 3800 years, an adiabatic wind terminal speed $V_{A\infty} = 2000$ km s^{-1} (which with $\eta_{he} = 0.1$ is reduced to $V_{\eta\infty} = 632.5$ km s^{-1}), lower and upper limits for the injected dust size distribution, $a_{min} = 0.0005 \mu\text{m}$ and $a_{max} = 0.05 \mu\text{m}$, respectively. The average conditions, gas density and temperature, for the thermalized medium in this case are $\langle n \rangle \sim 7.4 \text{ cm}^{-3}$ and $\langle T \rangle = 5.2 \times 10^6$ K. For typical supernova values ($M_{ej} = 8 M_{\odot}$, $E_{SN} = 10^{51}$ erg s^{-1}) and the prevailing conditions inside the cluster, evaluation of equation (4) results in an injection timescale $\tau_{inj} = 2800$ years, when the SN leading shock radius is about 4 pc and is well-contained inside R_{SC} . The main input parameters used in our four models are summarized in Table 2 and the derived quantities from the hydrodynamical model are presented in Table 3.

For NGC 604 and NGC 595, which stellar content is above $10^5 M_{\odot}$ and the estimated age is ~ 4 Myr (Relaño et al. 2013), the radiation field emerging from them is assumed to be 10^6 and 5×10^5 times that of the solar neighborhood, while for regions with stellar masses lying below $10^5 M_{\odot}$, the radiation field is assumed to be 2×10^5 and 10^5 times the solar neighborhood radiation field, respectively. In all our models, dust emission in the thermalized medium is dominated by collisional

TABLE 2
INPUT PARAMETERS

| Region | L_{SC} (10^{39} erg s $^{-1}$) | η_{he} - | η_{ml} - | U - |
|---------|---|------------------|------------------|-----------------|
| NGC 604 | 17.1 | 0.1 | 0 | 1×10^6 |
| NGC 595 | 6.72 | 0.1 | 0 | 5×10^5 |
| NGC 588 | 2.05 | 0.1 | 1 | 2×10^5 |
| NGC 592 | 1.19 | 0.1 | 1 | 1×10^5 |

NOTE. — The Table presents the input parameters we used for the selected clusters. The values of L_{SC} were obtained from the relation $L_{SC} = 3 \times 10^{39} (M_{SC}/10^3 M_{\odot})$ erg s $^{-1}$ (Leitherer et al. 1999). U characterizes the strength of the radiation field in multiples of the solar neighborhood value, J_{λ}^{NBH} (Mathis et al. 1983).

TABLE 3
MODEL OUTPUTS

| Region | $V_{\eta\infty}$ (km s $^{-1}$) | $\langle n \rangle$ (cm $^{-3}$) | $\langle T \rangle$ (10^6 K) | $\tau_{inj}^{(m)}/\langle \Delta\tau_{SN} \rangle$ - |
|---------|-------------------------------------|--------------------------------------|------------------------------------|---|
| NGC 604 | 630 | 7.4 | 5.2 | 0.50 |
| NGC 595 | 630 | 2.9 | 5.3 | 0.50 |
| NGC 588 | 450 | 2.5 | 2.6 | 0.15 |
| NGC 592 | 450 | 1.5 | 2.6 | 0.10 |

NOTE. — The values of $V_{\eta\infty}$ were obtained from an $V_{A\infty} = 2000$ km s $^{-1}$ and the corresponding assumed values of η_{he} and η_{ml} presented in Table 2. The average gas densities and temperatures were obtained from the hydrodynamical star cluster wind model. Finally, we present the ratio of the dust injection timescale to the average interval between successive supernova explosions in the star cluster.

heating at NIR wavelengths, while photon heating at MIR wavelengths. We also note that in a coeval cluster, the number of UV photons starts to drop (as $\sim t^{-5}$, Beltrametti et al. 1982) as a consequence of the explosion of the massive stars (Martínez-González et al. 2014). For simplicity, all of the modeled clusters are assumed to be contained in the same volume. The average density and temperature inside the cluster in each case are shown in Table 3.

3.1. The Cold, Warm Dust and PAHs Components

Following Relaño et al. (2016), we have used three additional components to account for the observed infrared spectral energy distributions. These components arise from the H II regions surrounding the central star clusters. One component is that from cold dust radiating at low temperatures (a few times ~ 10 K). From this component a huge amount of dust can be inferred (thousands or tens of thousands of solar masses), most probably the result of efficient grain growth (see for example Asano et al. 2013). A second component corresponds to warm dust ($\sim (50 - 100)$ K) which Relaño et al. (2016) attributes to the emission of very small grains. The third component is that from Polycyclic Aromatic Hydrocarbons (PAHs). The heating of this grains is always dominated by the absorption of the radiation field, while collisional heating is always negligible due the low temperature of the diffuse medium in which the grains are immersed. For simplicity, in fitting the observed data

in the case of the warm and cold components, we have followed the approach taken by Mattsson et al. (2015). In their approach, one assumes a dust temperature distribution instead of a dust size distribution (for the hot dust component we did the opposite). With the method, one does not have to assume a certain radiation field to derive a dust mass. Our chosen dust temperature distribution is represented by a power-law of the form $G(a, T_d) \propto T_d^{-3-\chi/2}$, where χ is the effective emissivity index which we take as 1.

For the cold and warm dust components, we have set the limits of the size distribution to $0.0001 \mu\text{m}$ and $0.5 \mu\text{m}$ for all the models. The temperature range for our NGC 604 and NGC 595 cold dust models was set to $(16 - 33)$ K, while for the NGC 588 and NGC 592 models it was set to $(12 - 33)$ K. In the case of the warm dust component the range of temperatures is $(50 - 100)$ K for all the models. Finally, for the PAHs component, the range of sizes was taken from $0.0001 \mu\text{m}$ to $0.0009 \mu\text{m}$ while the range of temperatures was set to $(90 - 750)$ K in all the models.

4. RESULTS

In Figure 3, we show the evolution of the total mass of dust within the central star cluster ($\leq R_{SC}$) as a result of successive supernova explosions. The mass of dust produced in the ejecta of individual supernovae is taken to be ~ 0.8 (the amount of dust already produced in SN 1987A), 0.5 , 0.1 and $0.5 M_{\odot}$ for our NGC 604, NGC 595, NGC 588 and NGC 592 models, respectively. For the NGC 588 and NGC 592 models, one can note that due to the extreme conditions in the thermalized ISM leading to a rapid sputtering of the grains and a long interval between SNe, the mass of dust remaining in the cluster as a result of a single injection event becomes negligible after a few thousand years. If the dust injection timescale is comparable to the interval between supernova explosions, then there is a non-negligible amount of dust present in the cluster during a large fraction of the supernova era (which lasts the order of $\sim 4 \times 10^7$ years).

Figure 4 shows the calculated IR SEDs for our NGC 604 model at three different evolutionary times (300, 2800 and 3800 years) for a total of $0.8 M_{\odot}$ of dust condensed in the supernova ejecta. For ease of comparison, we show the four separate components required to fit the observations, in a similar fashion as Relaño et al. (2016). These evolutionary times were selected because at ~ 300 years, the emission at $3.6 \mu\text{m}$ from the unshocked and shocked ejecta are approximately equal and thus the total emission is at a local maximum, and at ~ 2800 years when the incorporation of all the dust into the thermalized medium has been completed. Before ~ 300 years, the emission arising from dust in the unshocked ejecta is dominant over the emission corresponding to dust in the thermalized medium. After ~ 2800 years, the emission drops fast (as a consequence of rapid grain destruction) until ~ 3800 years, when the second injection event starts, as shown in panel d in Figure 4.

We ought not to omit that the contribution from starlight in the infrared SEDs is orders of magnitude below the observed data points and therefore it is not responsible for the infrared excesses we are devoted to explain. At 300 and 2800 years after the start of the first injection event, the presence of the NIR-MIR excess with respect to the PAHs emission is evident. Only at ~ 3800 years, the ex-

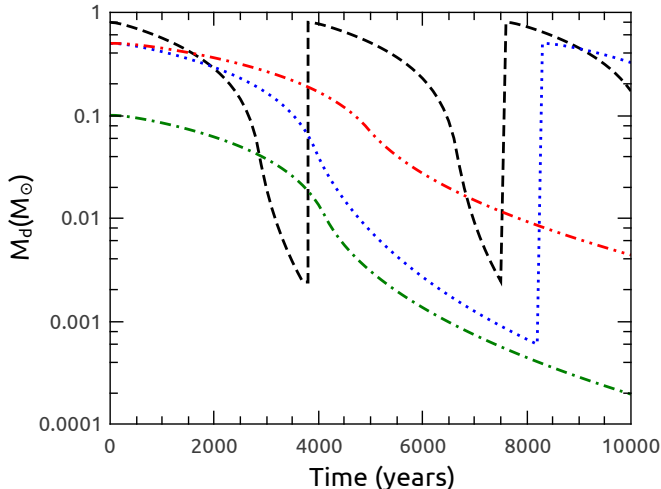


FIG. 3.— The evolution of the dust mass in the star cluster. The curves display the total mass of dust present in the star cluster as a function of time for our NGC 604 (black dashed line), NGC 595 (blue dotted line), NGC 588 (green dash-dotted line) and NGC 592 (red dash-double dotted line) models. In the models, the mass of dust injected inside the star cluster is 0.8, 0.5, 0.1 and 0.5 M_{\odot} , respectively. Note that almost all the dust mass is returned to the gas phase in a timescale of a few thousand years as a result of efficient thermal sputtering.

cess is marginal. In general the presence of the NIR-MIR excess should be detectable for $\sim 85\%$ of the time spent by the cluster in the supernova era with the assumed supernova rate and heating efficiency (10%). This percentage is calculated from the time during which the dust emission has a clear excess with respect to the emission of PAHs, not with the agreement with the observed data of a particular cluster in a particular evolutionary stage. In this case, the mass of gas enclosed in the star cluster ($\leq R_{SC}$) is 535 M_{\odot} , ~ 107 times more than the typical SN ejecta mass we have assumed.

Our calculated IR SEDs for the NGC 595 for the selected evolutionary times are presented in Figure 5. In this case, a total dust mass of 0.5 M_{\odot} was used. One can observe that the agreement with the observed data points is excellent at 1000 and 3800 years, while for 8000 years the excess with respect to the emission of PAHs is absent. However, the NIR-MIR infrared excess associated to these grains would be detectable during $\sim 60\%$ of the evolution of the cluster in this model (see panel d in Figure 5). In this model the mass of gas in the star cluster is 210 M_{\odot} .

For our NGC 588 model (evaluated and displayed in Figure 6) we used 0.1 M_{\odot} of injected dust, the infrared emission behaves similarly to the previous cases at 1000 and 4000 years. At 10000 years the grain emission is overcome by the PAHs emission and the NIR-MIR excess of our interest is absent. Only during $\sim 20\%$ of the supernova era the NIR-MIR excess would be present as shown in the comparison for the modeled and observed flux at 3.6 μm in Figure 6. In this case, the enclosed mass of gas in the star cluster is 180 M_{\odot} .

In the case of NGC 592 (see Figure 7), the results in general are very similar to the case of NGC 588 for the three shown evolutionary times even though this cluster is less massive and the assumed amount of dust injected within the star cluster is 0.5 M_{\odot} . The stellar mass of NGC

592 is roughly the same as some other prominent clusters in M33 like IC 131 and IC 131-West (Relaño et al. 2010). For this reason, we will use them as probes for the evolutionary trend resultant from the injection and destruction of grains. For our NGC 592, the star cluster contains 106 M_{\odot} of gas.

In Figure 8, the observed IR SEDs for NGC 592 (squares filled with cyan), IC 131 (pink stars) and ICI 131-West (green diamonds) are shown. Other interesting regions identified by Relaño et al. (2013) are regions 20 and 85. Region 20 (in the following referred as SSC20) shows strong emission in excess to that of PAHs (yellow circles in Figure 8), whereas the excess is absent for region 85 (referred as SSC85). In the plot, we have overlaid our predicted IR SEDs for the NGC 592 model evaluated at 1000, 4800, 6000 and 10000 years.

In the frame of our models, the differences between these five clusters at short wavelengths ($\leq 10 \mu\text{m}$) might be explained by considering supernova dust injections at different evolutionary stages, off-centered supernovae (evolving in the blowout regime as explained by Tenorio-Tagle et al. (2015a) and Silich & Tenorio-Tagle (2017)) and/or simply supernovae with different dust yields.

5. DUST FROM OTHER SOURCES

As pointed out earlier in this paper, before the first supernova occurs (at ~ 3.5 Myr), the intracluster medium is already thermalized by the interaction of the stellar winds of individual stars, leading to the launching of a fast outflow, the star cluster wind (e.g. Chevalier & Clegg 1985; Cantó et al. 2000; Silich et al. 2004). Therefore, at the time of the first SNe, any residual dust left over from star formation should have been, either destroyed in the hot wind or expelled out of the cluster. In the latter case, far from the bulk of the stars and in a less hot and less dense medium, the expelled dust must be contributing to the emission which is accounted as the warm dust component (green dotted curves in Figures 4 to 7).

Dust condensed out of the material injected by Wolf-Rayet stars (WR) must also contribute to the IR emission in the clusters; however, their contribution to the total dust budget is unclear and most likely minor compared to dust injection by SNe (e.g. Matsuura et al. 2013, for the case of the Small Magellanic Cloud). Moreover, clusters with a presumably large WR population producing some amount of dust, show no NIR-MIR excess (e.g. SSC85), making WR stars unlikely to play a significant role in producing the excess.

6. SUMMARY

Here we have considered the infrared emission of the dust grains formed in core-collapse SN within young massive stellar clusters. It is noted that the emission at NIR-MIR wavelengths is more likely to be produced by stochastically-heated small grains and that several effects can prevent their fast destruction. As a result, the period during which their emission dominates over the foreground PAHs features is enhanced. These effects can be summarized as follows:

1. Magnetohydrodynamic turbulence in star clusters (Hirashita et al. 2010), together with the compression of the magnetic field lines (Shull 1977), acting

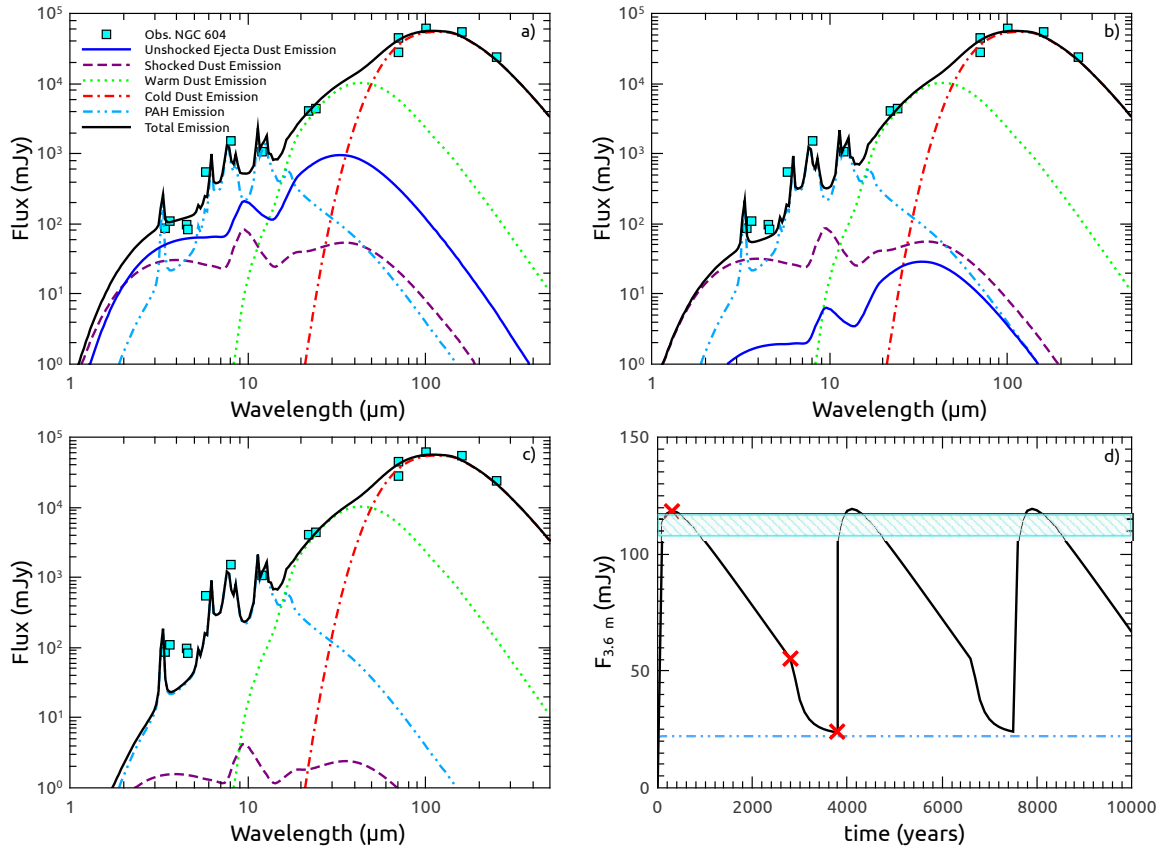


FIG. 4.— The infrared spectral energy distribution for our NGC 604 dust emission model at 300 (panel a), 2800 (panel b) and 3800 (panel c) years after the first injection event started with an interval between events ~ 3800 years. The blue-solid and purple-dashed lines depict the emission from dust residing in the unshocked and shocked ejecta, respectively, for our NGC 604 model. The dash-double dotted blue, dotted-green and dash-dotted red lines correspond to the emission of pre-existing PAHs, warm and cold grains in the illuminated H II region associated to the central cluster, respectively. Total emission is displayed as a black solid line. Observed values (squares in cyan) were obtained from the tables provided in Relaño et al. (2016). Panel d (bottom right) presents the evolution of the flux modeled at $3.6 \mu\text{m}$ as compared to the observed value (shaded region in cyan, which includes the associated observational error) and the emission from PAHs (dash-dotted light blue line). The red crosses in panel d indicate the times displayed in the other panels.

in clumpy SN ejecta may enhance the occurrence of grain-grain collisions, producing an excess of small grains (Jones et al. 1996), we thus consider that the grain population is formed only by grains with radii $\lesssim 0.05 \mu\text{m}$.

2. Small grains can actually be traversed by colliding ions if these are energetic enough not to be stopped inside the small dust particles, as shown by Serra Díaz-Cano & Jones (2008). This effect reduces the derived sputtering rates for very small grains thus increasing their lifetimes.
3. The NIR-MIR infrared excesses are more persistent if the time required to shock-process individual SN ejecta (Tang & Wang 2009) is comparable to the interval between SN explosions.
4. A low efficiency in the thermalization of the kinetic energy of stellar winds and supernova explosions (Silich et al. 2007, 2009) would also alleviate the destruction of grains of all sizes.
5. Star clusters with modest masses ($\sim 10^4 M_{\odot}$), if not mass-loaded, may struggle with the capture and interaction of SN ejecta, thus inhibiting the driving of a smooth wind in the sense of the Chevalier & Clegg (1985) classical model; hence,

the consideration of mass-loaded winds is also crucial in these cases.

7. CONCLUDING REMARKS

We have applied our SN dust injection model to the four most prominent star clusters in the M33 galaxy, spanning a wide range of masses and dust (from different sources) contents, from the Relaño et al. (2013, 2016) sample of H II regions and their associated observed infrared SEDs. We found that massive clusters, like NGC 604 and NGC 595, should exhibit NIR-MIR excesses during a significant fraction of their evolution, especially if the heating efficiency of the thermalized matter is low as suggested by several independent studies (e.g. Smith et al. 2006; Silich et al. 2009). With regard to star clusters with masses of a few times $\sim 10^4 M_{\odot}$, we propose that the evolutionary trends of the NIR-MIR emission obtained from our models is well represented by NGC 592, NGC 592, IC 131 and IC 131-West, which have similar masses and their emission at wavelengths $\geq 10 \mu\text{m}$ is almost identical. When analyzing other young massive clusters with no available stellar mass estimates, e.g. the star clusters with identification numbers 20 and 85 in the Relaño et al. (2016) sample, one can observe that while the emission at wavelengths $\geq 10 \mu\text{m}$ is very similar to that found in NGC 588, NGC 592, IC 131 and IC 131-West, they differ at short wavelengths by an order

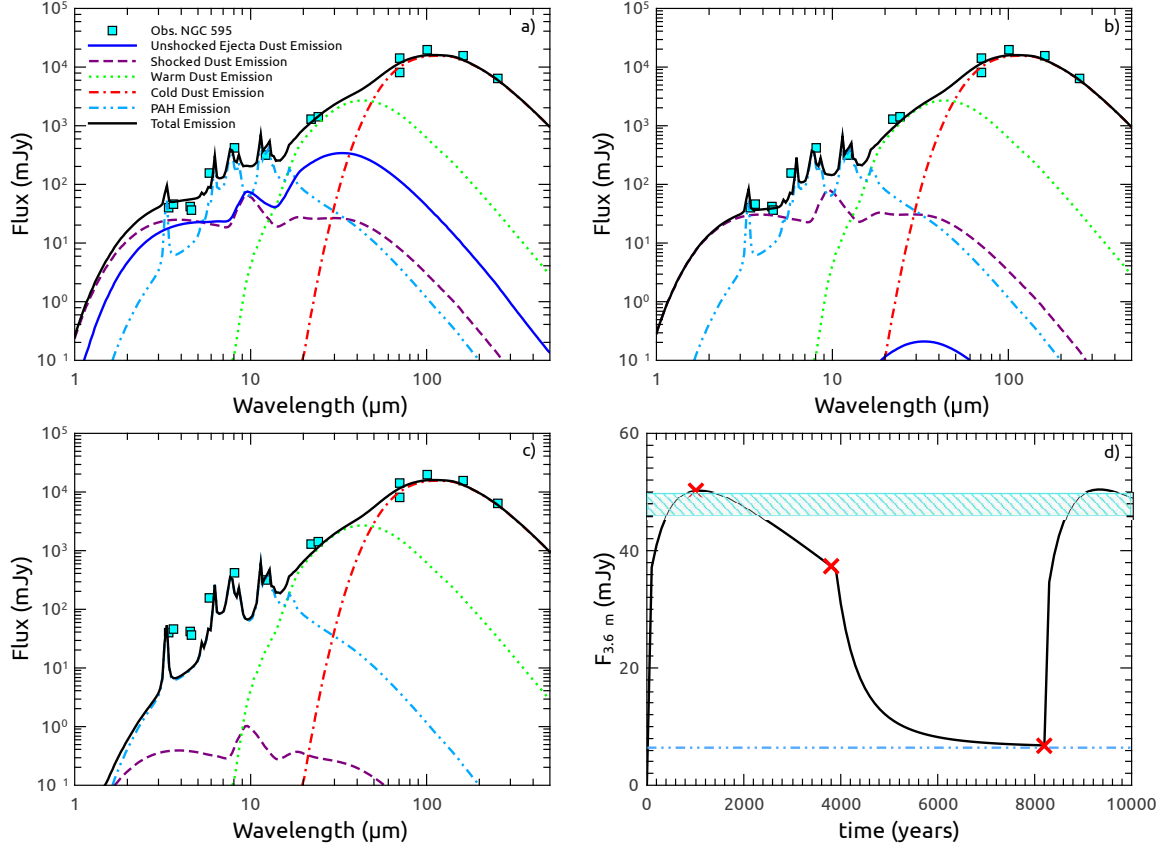


FIG. 5.— Same as Figure 4 but for the model representing NGC 595. In this case, the mass of the stellar cluster is $2.24 \times 10^5 M_{\odot}$. Relevant evolutionary times in this case are 1000, 3800 and 8200 years.

of magnitude. We interpret this as evidence that region 20 experienced grain injection from a supernova in the last few thousand years, whereas region 85 should not have had a recent grain injection occurring at its central region.

Our model thus predicts that a NIR-MIR excess might be transiently observed in the spectra of young massive star clusters. The characteristic timescale for such an excess to be observed and thus the probability to observe it in a sample of the selected clusters depends on the ability to capture the ejecta of individual supernovae inside the clusters. In broad terms, the presence of the NIR-MIR excess is an indication of efficient dust production by SNe exploding within star clusters. It also suggests the presence of a large population of very small grains heated to high temperatures as well as strong grain destruction

by ionic collisions.

Further analysis of the implications of the blowout scenario (Tenorio-Tagle et al. 2015a; Silich & Tenorio-Tagle 2017) on the survival, manifestation and dispersal of supernova-produced dust grains is left for a future communication.

The authors thank G. Tenorio-Tagle, S. Silich and the anonymous Referee for their careful reading and helpful suggestions which greatly improved the paper, and M. Relaño for answering our questions about her data. Support for this project was provided by the Czech Science Foundation grant 209/15/06012S and by project RVO: 6785815. SMG also thanks initial support for the project provided by INAOE and CONACYT, México through research grant 167169. SMG dedicates this work to the memory of his beloved baby Andél.

REFERENCES

- Arendt, R. G., Dwek, E., Blair, W. P., et al. 2010, *ApJ*, 725, 585
 Asano, R. S., Takeuchi, T. T., Hirashita, H., & Nozawa, T. 2013, *MNRAS*, 432, 637
 Beltrametti, M., Tenorio-Tagle, G., & Yorke, H. W. 1982, *A&A*, 112, 1
 Bevan, A., Barlow, M. J., & Milisavljevic, D. 2016, *ArXiv e-prints*, arXiv:1611.05006
 Bianchi, S., & Schneider, R. 2007, *MNRAS*, 378, 973
 Biscaro, C., & Cherchneff, I. 2016, *A&A*, 589, A132
 Bocchio, M., Marassi, S., Schneider, R., et al. 2016, *A&A*, 587, A157
 Bocchio, M., Micelotta, E. R., Gautier, A.-L., & Jones, A. P. 2012, *A&A*, 545, A124
 Cantó, J., Raga, A. C., & Rodríguez, L. F. 2000, *ApJ*, 536, 896
 Cernuschi, F., Marsicano, F., & Codina, S. 1967, *Annales d'Astrophysique*, 30, 1039
 Chevalier, R. A., & Clegg, A. W. 1985, *Nature*, 317, 44
 De Looze, I., Barlow, M. J., Swinyard, B. M., et al. 2017, *MNRAS*, 465, 3309
 Draine, B. T., & Salpeter, E. E. 1979, *ApJ*, 231, 77
 Dwek, E. 1986, *ApJ*, 302, 363
 Dwek, E. 1987, *ApJ*, 322, 812
 Dwek, E., & Arendt, R. G. 1992, *ARA&A*, 30, 11
 Freedman, W. L., Madore, B. F., Gibson, B. K., et al. 2001, *ApJ*, 553, 47

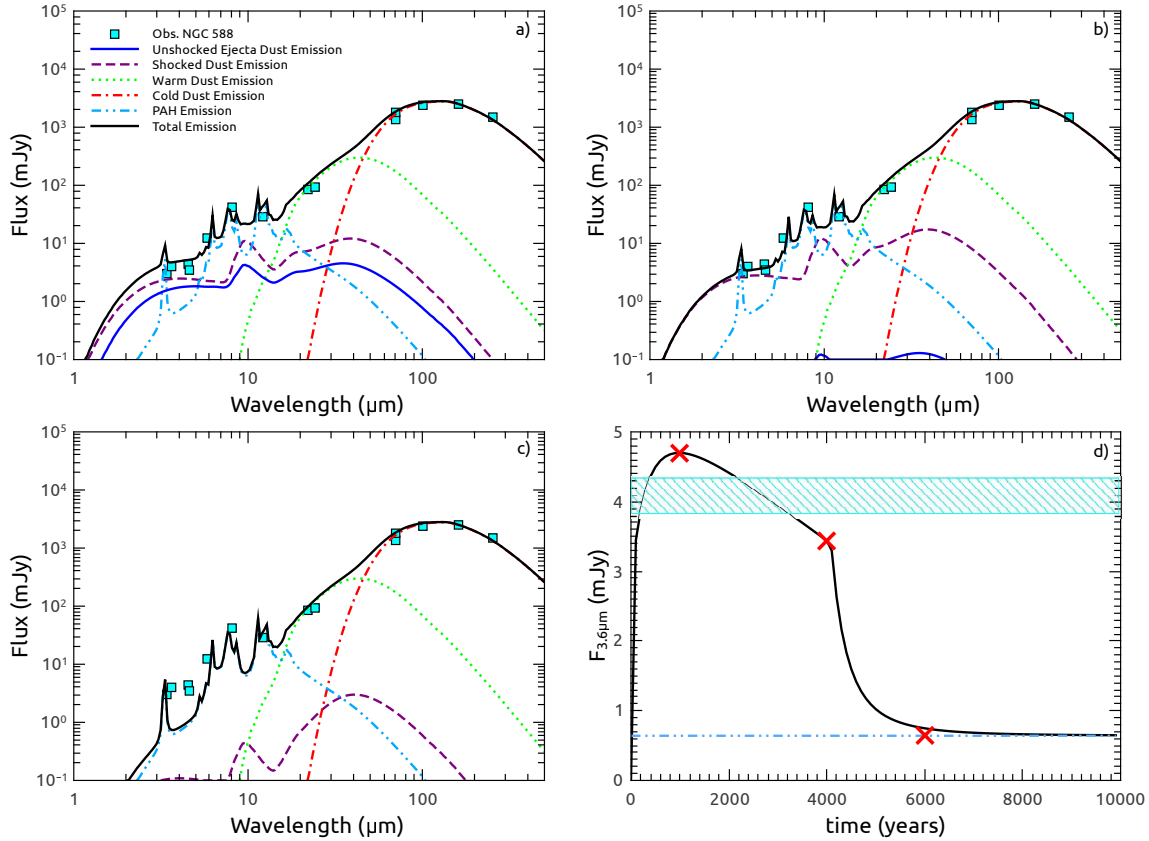


FIG. 6.— Same as Figure 4 but for the model representing NGC 588. In this case, the mass of the stellar cluster is $6.86 \times 10^4 M_{\odot}$. Panels a, b and c show the calculated fluxes $3.6 \mu\text{m}$ at 1000, 4000 and 10000 years.

Ghavamian, P., & Williams, B. J. 2016, ArXiv e-prints, arXiv:1608.03373
 Gordon, S. M., Kirshner, R. P., Duric, N., & Long, K. S. 1993, ApJ, 418, 743
 Grenman, T., Gahm, G. F., & Elfegren, E. 2017, A&A, 599, A110
 Guhathakurta, P., & Draine, B. T. 1989, ApJ, 345, 230
 Hirashita, H., Nozawa, T., Yan, H., & Kozasa, T. 2010, MNRAS, 404, 1437
 Indebetouw, R., Matsuura, M., Dwek, E., et al. 2014, ApJ Lett, 782, L2
 Izotov, Y. I., Guseva, N. G., Fricke, K. J., Krügel, E., & Henkel, C. 2014, A&A, 570, A97
 Jones, A. P., Tielens, A. G. G. M., & Hollenbach, D. J. 1996, ApJ, 469, 740
 Krause, M., Charbonnel, C., Decressin, T., Meynet, G., & Prantzos, N. 2013, A&A, 552, A121
 Kroupa, P. 2001, MNRAS, 322, 231
 Lakićević, M., van Loon, J. T., Meixner, M., et al. 2015, ApJ, 799, 50
 Laor, A., & Draine, B. T. 1993, ApJ, 402, 441
 Larsen, S. S., Origlia, L., Brodie, J. P., & Gallagher, J. S. 2006, MNRAS, 368, L10
 Lau, R. M., Herter, T. L., Morris, M. R., Li, Z., & Adams, J. D. 2015, Science, 348, 413
 Leitherer, C., Schaerer, D., Goldader, J. D., et al. 1999, ApJS, 123, 3
 Marassi, S., Schneider, R., Limongi, M., et al. 2015, MNRAS, 454, 4250
 Martínez-González, S., Silich, S., & Tenorio-Tagle, G. 2014, ApJ, 785, 164
 Martínez-González, S., Tenorio-Tagle, G., & Silich, S. 2016, ApJ, 816, 39
 Mathis, J. S., Mezger, P. G., & Panagia, N. 1983, A&A, 128, 212
 Matsuura, M., Woods, P. M., & Owen, P. J. 2013, MNRAS, 429, 2527
 Matsuura, M., Dwek, E., Barlow, M. J., et al. 2014, ArXiv e-prints, arXiv:1411.7381

Mattsson, L., Gomez, H. L., Andersen, A. C., & Matsuura, M. 2015, MNRAS, 449, 4079
 Meynet, G., & Maeder, A. 2003, A&A, 404, 975
 Meynet, G., Maeder, A., Schaller, G., Schaerer, D., & Charbonnel, C. 1994, A&AS, 103
 Micelotta, E. R., Dwek, E., & Slavin, J. D. 2016, A&A, 590, A65
 Moseley, S. H., Dwek, E., Glaccum, W., Graham, J. R., & Loewenstein, R. F. 1989, Nature, 340, 697
 Nozawa, T., Kozasa, T., Habe, A., et al. 2007, ApJ, 666, 955
 Nozawa, T., Kozasa, T., Umeda, H., Maeda, K., & Nomoto, K. 2003, ApJ, 598, 785
 Palouš, J., Wunsch, R., Martínez-González, S., et al. 2013, ApJ, 772, 128
 Raymond, J. C., Cox, D. P., & Smith, B. W. 1976, ApJ, 204, 290
 Reines, A. E., Johnson, K. E., & Hunt, L. K. 2008, AJ, 136, 1415
 Relaño, M., Monreal-Ibero, A., Vílchez, J. M., & Kennicutt, R. C. 2010, MNRAS, 402, 1635
 Relaño, M., Verley, S., Pérez, I., et al. 2013, A&A, 552, A140
 Relaño, M., Kennicutt, R., Lisenfeld, U., et al. 2016, ArXiv e-prints, arXiv:1606.03624
 Rémy-Ruyer, A., Madden, S. C., Galliano, F., et al. 2015, A&A, 582, A121
 Reynolds, S. P., & Chevalier, R. A. 1984, ApJ, 278, 630
 Sarangi, A., & Cherchneff, I. 2015, A&A, 575, A95
 Serra Díaz-Cano, L., & Jones, A. P. 2008, A&A, 492, 127
 Sharma, P., Roy, A., Nath, B. B., & Shchekinov, Y. 2014, MNRAS, 443, 3463
 Shull, J. M. 1977, ApJ, 215, 805
 Silich, S., Bisnovatyi-Kogan, G., Tenorio-Tagle, G., & Martínez-González, S. 2011, ApJ, 743, 120
 Silich, S., & Tenorio-Tagle, G. 2017, MNRAS, 465, 1375
 Silich, S., Tenorio-Tagle, G., & Muñoz-Tuñón, C. 2007, ApJ, 669, 952
 Silich, S., Tenorio-Tagle, G., & Rodríguez-González, A. 2004, ApJ, 610, 226
 Silich, S., Tenorio-Tagle, G., Torres-Campos, A., et al. 2009, ApJ, 700, 931

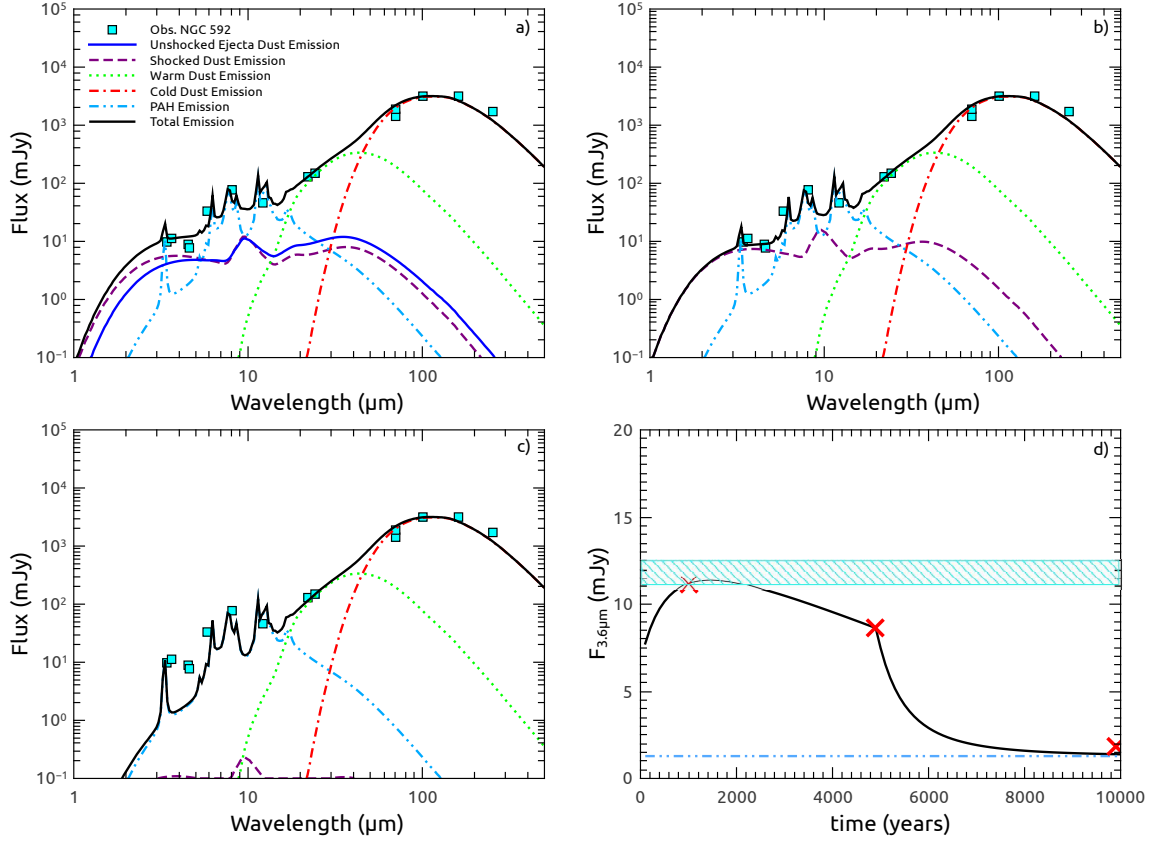


FIG. 7.— Same as Figure 4 but for the model representing NGC 592. In this case, the mass of the stellar cluster is $3.98 \times 10^4 M_{\odot}$. Panels a, b and c show the calculated flux at 1000, 4800 and 10000 years.

Smith, L. J., Westmoquette, M. S., Gallagher, J. S., et al. 2006, *MNRAS*, 370, 513
 Suntzeff, N. B., & Bouchet, P. 1990, *AJ*, 99, 650
 Tabatabaei, F. S., Beck, R., Krügel, E., et al. 2007, *A&A*, 475, 133
 Takeuchi, T. T., Hirashita, H., Ishii, T. T., Hunt, L. K., & Ferrara, A. 2003, *MNRAS*, 343, 839
 Tang, S., & Wang, Q. D. 2005, *ApJ*, 628, 205
 Tang, S., & Wang, Q. D. 2009, *MNRAS*, 397, 2106
 Temim, T., & Dwek, E. 2013, *ApJ*, 774, 8
 Tenorio-Tagle, G., Muñoz-Tuñón, C., Silich, S., & Cassisi, S. 2015a, *ApJ Lett*, 814, L8
 Tenorio-Tagle, G., Silich, S., Martínez-González, S., et al. 2013, *ApJ*, 778, 159
 Tenorio-Tagle, G., Silich, S., Martínez-González, S., Terlevich, R., & Terlevich, E. 2015b, *ApJ*, 800, 131
 Tielens, A. G. G. M., McKee, C. F., Seab, C. G., & Hollenbach, D. J. 1994, *ApJ*, 431, 321

Todini, P., & Ferrara, A. 2001, *MNRAS*, 325, 726
 Tsai, J. C., & Mathews, W. G. 1995, *ApJ*, 448, 84
 Vanzani, L., Hunt, L. K., Thuan, T. X., & Izotov, Y. I. 2000, *A&A*, 363, 493
 Weaver, R., McCray, R., Castor, J., Shapiro, P., & Moore, R. 1977, *ApJ*, 218, 377
 Wunsch, R., Palouš, J., Tenorio-Tagle, G., & Ehlerová, S. 2017, *ApJ*, 835, 60
 Wunsch, R., Silich, S., Palouš, J., Tenorio-Tagle, G., & Muñoz-Tuñón, C. 2011, *ApJ*, 740, 75
 Yadav, N., Mukherjee, D., Sharma, P., & Nath, B. B. 2016, *ArXiv e-prints*, arXiv:1603.00815
 Yamada, K., & Kitayama, T. 2005, *PASJ*, 57, 611
 Yan, H., Lazarian, A., & Draine, B. T. 2004, *ApJ*, 616, 895
 Yang, H., Chu, Y.-H., Skillman, E. D., & Terlevich, R. 1996, *AJ*, 112, 146

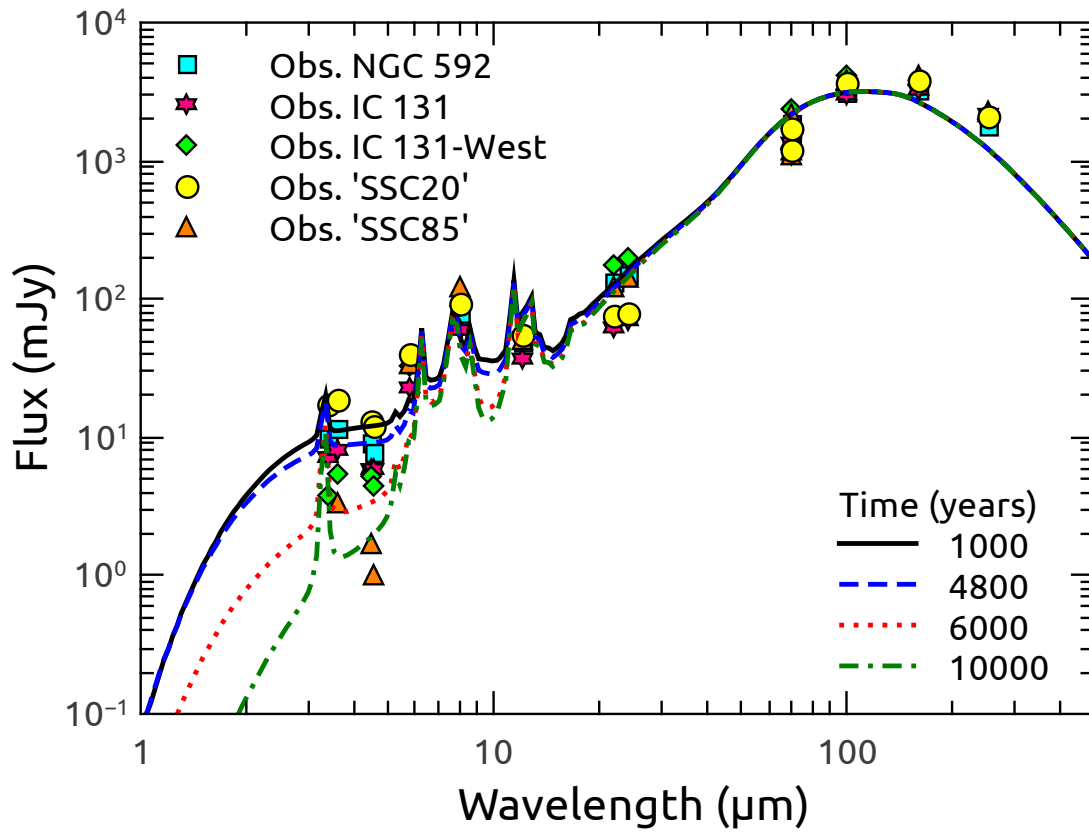


FIG. 8.— Infrared SEDs for regions NGC 592, IC 131, IC 131-West, SSC20 and SSC85. We have overlaid the predictions for our NGC 592 model at 1000 (solid blue line), 4800 (blue dashed line), 6000 (red dotted line), and 10000 (green dash-dotted line) years, respectively.